Wooden building damage analysis in Mashiki town for the 2016 Kumamoto earthquakes on April 14 and 16

Masumi Yamada,[a] Junzo Ohmura,[b] and Hiroyuki Goto[c]

The 2016 Kumamoto earthquakes caused serious building damage in Mashiki town. Since two large earthquakes occurred within an interval of 28 hours, it is difficult to separate the damage caused by each of these earthquakes. We analyzed aerial photos of the center of Mashiki town taken before and after the second event, which allow us to separate the damage due to the two earthquakes. Our analysis shows that building damage was concentrated especially on the river terrace of the Akitsu river, and there were almost no collapsed buildings in the south of the damaged area. The pattern of damage distribution of the two events was similar, which suggests that the damage to the wooden buildings was caused by local conditions. The analysis of past aerial photos showed that the heterogeneity of the damage distribution is difficult to explain by only the building age. The cause of this heterogeneity was found to be not due to an earthquake faulting effect, but due to a combination of building seismic performance and local site conditions.

INTRODUCTION

The 2016 Kumamoto earthquake sequence consists of two major earthquakes that occurred in Kumamoto, located in the southern part of Japan, in April 2016. The first earthquake occurred at 21:26 on April 14. The focal depth was 11 km, the JMA (Japan Meteorological Agency) magnitude was 6.5, and the highest JMA seismic intensity recorded was 7 in Mashiki town (Japan Meteorological Agency, 2016). The second and larger earthquake occurred 28 hours after the first event, at 01:25 on April 16. The focal depth was 12 km, the JMA magnitude was 7.3, and the highest JMA seismic intensity recorded was also 7 in Mashiki town (Japan Meteorological Agency, 2016).

Mashiki town, located about 10 km northeast of the epicenters, was heavily damaged by

[a] DPRI, Kyoto University, Gokasho, Uji, 611-0011, Japan
[b] Bukkyo University, 96, Kitahananobo-cho, Murasakino, Kita-ku, Kyoto, 603-8301, Japan
[c] DPRI, Kyoto University, Gokasho, Uji, 611-0011, Japan

these earthquakes, and 7 and 12 people were killed in the town after the first and second earthquakes, respectively, due to the collapse of houses (Nishinippon Shimbun Website, 2016). As there was only 28 hours between the earthquakes, it is difficult to separate the damage resulting from each of the two earthquakes.

In this study, we analyzed aerial photos taken before, after, and during the interval of the two events (Geospatial Information Authority of Japan, 2016a), which allowed us to separate the damage due to the earthquakes on April 14 and 16. We compared these photos and identified the distribution of collapsed buildings for the two earthquakes. We then compared these results to field survey results to confirm the accuracy of the photo analysis. Finally, we discussed the cause of the heterogeneous damage distribution, such as fault surface rupture, subsurface soil amplification, and the seismic performance of buildings.

EARTHQUAKES AND STRONG MOTION

Figure 1 shows the JMA seismic intensity and aftershock distribution for the April 16 event. The main fault trends in the SW–NE direction (Yagi et al., 2016; Asano and Iwata, 2016). Strong motions were recorded along the fault, especially in Mashiki town and Nishihara village, where the recorded shaking intensity was 7, which is the highest intensity rating on the JMA scale. Small surface rupture (40 cm) was observed at the center of Mashiki town (Geospatial Information Authority of Japan, 2016a; Goda et al., 2016), indicated by the red lines shown in Figure 2. Therefore, the closest distance to the fault was less than 1 km from the center of Mashiki.

Figure 3 shows the horizontal velocity waveforms for the April 14 and 16 events (Japan Meteorological Agency, 2016; NIED, 2016) and the locations of the stations are shown in Figure 2. Strong motions of the April 16 event are larger than those of the April 14 event; the PGVs at Mashiki townhall are 135 and 176 cm/s for the April 14 and 16 events, respectively. Figure 2 also shows the seismic intensity recorded at these stations in square symbols. The intensity was 6.5 at the KiK-net Mashiki station in the northern part of the town with higher elevation, and 6.8 at Mashiki townhall. Note that all intensities shown are for the JMA scale, and were computed from the strong motion records. JMA intensity 7 corresponds to 11-12 on the MMI scale (Kunugi, 2000).

This ground motions are larger than the design level in the Japanese building standard law. The pseudo velocity response spectrum at Mashiki townhall is larger than the design spectrum at periods greater than 0.5 s for both the April 14 and 16 events and more than twice as large as the design level at 1–1.5 s (Committee to analyze causes of building damage in the Kumamoto earthquake, 2016). Therefore, severe damage would be expected in Mashiki town.

The geographical condition of the area is the floodplain and river terrace of the Akitsu river (Figure 4). The town was already developed in the Meiji era along Route 28 in the EW direction on the river terrace, and the lower floodplain was used as rice fields (Nagaki et al., 2009). In the 1970s, the village was expanded in the NS direction, and the lower floodplain was also used as residential areas. In recent times, all of the floodplain north of the Akitsu river has been developed as residential areas.

AERIAL PHOTO ANALYSIS

We used aerial photos of Mashiki town taken before and after the earthquakes to identify the collapsed buildings and age of the buildings. We also used a local house map (Zenrin Dijitown), which indicates the owners of houses and the usage of buildings in three categories (house, shop, other). We excluded housing complexes (such as apartments) from our analysis as these tend to be large structures. We focused on wooden structures and excluded structures constructed of other materials, such as steel and reinforced concrete structures. The structure type was estimated by considering the shape of the roof. In this study, we focused on the center of Mashiki town (north of the Akitsu river) shown in Figure 2.

DETECTION OF COLLAPSED BUILDINGS

The Geospatial Information Authority of Japan provided high-resolution aerial photos of Mashiki town on April 15 and 16, immediately after the two earthquakes (Geospatial Information Authority of Japan, 2016a). The photos covered the damaged area in Mashiki town shown in Figure 2, and allowed separating the damage due to the April 14 and 16 events. We compared these photos with the aerial image appearing on Google Earth, and visually detected collapsed buildings from each photo. We defined the following conditions to determine whether a building was collapsed: 1) the edge of the building was distorted, 2) the centerline of the roof was tilted, or 3) debris was observed around the building.

ESTIMATION OF BUILDING AGE

In order to estimate the building age, we compared aerial photos taken in previous years. We obtained aerial photos of Mashiki town taken in 1967, 1975, 1982, 1986, 1997, and 2008 (Geospatial Information Authority of Japan, 2016b). These photos were compared with the current aerial view appearing on Google Earth to estimate the building age. In comparing a past photo with the view on Google Earth, we defined that the building appearing on Google Earth was constructed after the year when the past photo was taken if the roof had a new shape, or if the house did not appear in the past photo. The building construction year was thereby classified into the following periods: (1) before 1967, (2) 1967–1975, (3) 1975–1982, (4) 1982–1986, (5) 1986–1997, (6) 1997–2008, and (7) after 2008.

FIELD SURVEY

A joint team from Kyoto University, NEWJEC Inc., and the Building Research Institute conducted a field survey of damaged buildings in Mashiki town from June 10–13, 2016, two months after the earthquake (Yamada et al., 2016a,b; Hayashida et al., 2016). We used these results to confirm the accuracy of the damage distribution determined from our aerial photo analysis. The survey was conducted in the area between Route 28 and the Akitsu river shown in Figure 5. Aftershock observations were also carried out at the same time at eight sites.

DAMAGE SURVEY OF WOODEN STRUCTURES

The damage condition of each building was determined by the team according to the damage pattern chart for wooden structures proposed by Okada and Takai (2000). Using this criteria, the damage experienced by buildings was classified into four categories: D0 (no damage), D1–D3 (partially collapsed), D4 (totally collapsed), and D5 (story failure). D4 buildings have serious damage of structural elements, such as tilt of the structure, and cannot be used. D5 buildings have story failure, i.e., one or more stories or the whole building collapsed.

The team visually inspected the extent of the damage and recorded the damage levels on the local house map. They also recorded the usage of the structure (house, store, office, storage, etc.) and the structural type (wood, steel, RC, etc.). For consistency with our photo analysis, we focused on the field survey results for wooden structures other than housing complexes. The total number of surveyed buildings was 1,114 of which 73 non-wooden buildings were not used for the analysis.

AFTERSHOCK OBSERVATION

In order to understand the local site responses and estimate the shaking distribution for the earthquakes, the team installed seismometers and observed aftershocks during the period of the field survey. A combination of JEP-6A3 sensors made by Mitsutoyo and LS-8800 loggers made by Hakusan were used for the recordings. Three component accelerations were measured continuously at the eight sites, shown by the triangles in Figure 2. The sampling frequency was 200 Hz and the cut-off frequency of the high-cut filter was 30 Hz. The observed records include an earthquake occurring at 22:08 on June 12, with a JMA magnitude of 4.3 and a depth of 7 km. The seismic intensity recorded at Mashiki town hall was 1 for this earthquake.

RESULTS

DAMAGE DISTRIBUTION FROM PHOTOS AND FIELD SURVEY

Figures 6 and 7 show the damage distributions identified from the aerial photo analysis before and after the April 16 event. The color of each circle indicates the ratio of collapsed buildings within a radius of 50 m. Each circle constitutes a grid point with an interval of 0.00025° (about 25 m). The grid points with at least 10 buildings are shown in the figures.

We analyzed 2,915 buildings and identified 78 and 378 collapsed buildings after the April 14 and 16 events, respectively. Although the number of damaged buildings from the April 16 event was about four times more than that from the April 14 event, the pattern of the distribution of the damaged area was similar. The most heavily damaged parts were located in the northern part of the area between Route 28 and the Akitsu river.

Figure 5 shows the ratio of D5 (story failure) buildings to all buildings, detected from the field survey. The distribution of D5 buildings was in a good agreement with our photo analysis shown in Figure 7. This is consistent with our expectation that most of the collapsed buildings identified from the aerial photos were story-collapsed buildings.

We compared the damage condition of each building from the field survey and aerial photo analysis, and the results are shown in Table 1 (see also Figures 8, 9, and 10). The total number of buildings that surveyed by both the field survey and photo analysis was 1,041. The collapsed buildings identified from the photo analysis mostly correspond to the D5 buildings (202 out of 233 detections, 87%). However, there were a significant number of damaged buildings not detected from the aerial photos (79 buildings), or falsely determined as damaged (31 buildings). In general, D4 and D5 buildings are classified as totally collapsed buildings in the damage survey (Okada and Takai, 2000). Using this definition, there should have been 439 totally collapsed buildings (158 of D4 and 281 of D5), however, only 233 totally collapsed buildings were identified by the photo analysis. We checked the buildings that were classified as fully collapsed in our photo analysis but that were classified as D1–D3 (partially collapsed) in the field survey. Seven of these had serious damage to their roofs, which caused us to classify them as fully collapsed in the photo analysis. In addition, two of these were not accessible from the public road, so in the field survey the damage condition was determined from only one side of the buildings. The aerial photo showed substantial debris around the buildings, which suggested that the actual damage condition might have been more serious than that determined by the field survey. Therefore, one of the advantages of photo analysis is that certain aspects of building damage can be detected, which could not be seen in the field survey.

DAMAGE RATIO AND BUILDING AGE

Figure 11(a) shows the percentage of collapsed buildings according to different construction periods. The damage distribution identified from the aerial photo is used for this analysis. The age was estimated using the previous aerial photos, and the distribution in age of the buildings is shown in Figure 12. Figure 11(a) shows that there was a strong correlation between the building age and the collapse ratio, and that the older buildings had higher collapse ratios. The buildings over 50 years old had a very high collapse ratio of 40%. The number of buildings analyzed for the different periods is shown in Figure 11(b). The figure shows that many buildings were constructed in the 1970s and 1980s, but that new buildings have been continually constructed, even during the last 10 years.

Since the percentages of damaged buildings constructed between 1967 and 1986 were similar, we focused on the buildings constructed during this period to minimize the effect of the building age. Figure 13 shows the ratio of the collapsed buildings only for buildings constructed between 1967 and 1986. Note that only the grid points with more than five buildings are shown in the figure. The distribution is very similar to Figure 7, which suggests that the damage distribution was caused not only by the age of the buildings, but also by other local conditions.

STRONG MOTION DISTRIBUTION FOR THE AFTERSHOCK ON JUNE 12

The triangle symbols in Figure 2 show the seismic intensity for the Mj 4.3 aftershock that occurred on June 12. The observed intensity had a close correlation with the topography except for station S5. Stations S1 and S2, closest to the Akitsu river and considered to be located on thick sediments, recorded larger ground motions. Stations S7 and S8, at higher elevation, experienced smaller amplification and recorded smaller ground motions. Stations S3 and S6 have site properties that are intermediate between these two groups. The pattern of site amplifications was also clearly visible in the frequency domain. Figure 14 shows the Fourier amplitude spectra of the EW component for certain selected sites. S1 and S2 experienced higher amplification in the 1–2 Hz range compared to S7 and S8, while S3 and S6 experienced moderate amplification in the same frequency range.

DISCUSSION

We found that the damage distribution in Mashiki town was very heterogeneous, and heavy damage was concentrated in the northern part of the area between Route 28 and the Akitsu river. There were almost no collapsed buildings south of the damaged area, where we expected a larger site amplification since they are close to the river. This raises important questions regarding the possible causes of the heterogeneous damage from the Kumamoto earthquakes. The local level of damage is not strictly related to the soil stiffness of the sites.

The similarity of the pattern of damage after the April 14 and April 16 earthquakes, shown in Figures 6 and 7, respectively, suggests that the damage of the wooden structures was caused by the local conditions, such as the seismic performance of the buildings or the subsurface soil structures, rather than the effects from the earthquake source. Small surface ruptures (red lines shown in Figure 2) appeared after the April 16 event very close to the damaged area (Geospatial Information Authority of Japan, 2016a), but this surface rupture was not observed on April 15, during the interval between the April 14 and 16 events (Shirahama et al., 2016). Therefore, it is difficult to explain the similar pattern of damage distribution as due to the effects of the surface rupture, such as static deformation or the hanging wall effect. The age of the buildings is observed to have an effect on the damage distribution (Figure 11), but cannot completely explain all of the observed aspects in Figure 13. The figure shows that the heterogeneity exists even when the buildings are of similar age.

One of the possible interpretations is that this heterogeneity was caused by the difference in ground motions due to the different subsurface soil response. Figure 2 shows the site response for the aftershock on June 12. For this aftershock the site amplification is related to the softness of the soil conditions with stations S1 and S2 showing the strongest amplification. If the same pattern holds for the large earthquakes on April 14 and 16, we would expect to see the highest level of damage in the area of S1 and S2. However, the field survey indicates that the ground motions during the large earthquakes, at least in the frequency range causing structural damage, were smaller in the area of S1 and S2. This may be due to a nonlinear effect of the subsurface soil structure (Idriss and Seed, 1968). S1 and S2 stations are located on the floodplain (see Figure 4), in an area of thick sediments with low shear wave velocity in the subsurface soil. These soil structures may show nonlinear effects during strong shaking that reduce the amplification for strong shaking (Aki, 1993; Wen et al., 1994). Further investigation and analysis is necessary to confirm this assumption.

Estimating damage from remote sensing data, such as satellite photography, has been widely performed recently (Booth et al., 2011; Foulser-Piggott et al., 2016). Comparing the damage levels found in the field survey and photo analysis showed that photo analysis is a reasonable method to identify story-collapsed buildings (D5), but it is difficult to identify D4 buildings (tilted buildings without story collapse). Figure 15 shows examples of the damage level determined from the photo analysis and field survey. The story collapsed building in Figure 15(a) was easily identified by the aerial photo, but the damage of the tilted building in Figure 15(b) was not seen in the vertically taken photo, although it was very clear from the field survey. Using comparisons with the field survey, the number of totally collapsed buildings that were detected from the photo analysis, was about half the number observed in the field.

It is noteworthy that the building code for wooden structures was significantly altered in 1981 and 2000. Buildings constructed after these years have, in general, improved seismic performance in Japan. Committee to analyze causes of building damage in the Kumamoto earthquake (2016) showed the percentages of D5 buildings at the center of Mashiki were 28%, 9%, and 2% for the buildings before 1981, between 1981 and 2000, and after 2000, respectively. These numbers are in good agreement with our result in Figure 11(a). However, our results using a narrower period of the building age showed the effect of the changes of the building code was not as significant as the aging effect. The building age seems to have more influence on the seismic performance than the difference in the building code. Committee to analyze causes of building damage in the Kumamoto earthquake (2016) also reported that 70% of inspected wooden structures built after 1981 had insufficient metal joints. This may also be one of the reason why the effect of the building code on the seismic performance was not so clear.

The Kumamoto earthquakes represent a unique sequence with two strong shakings above the design level due to closely-spaced earthquakes in both time and space. Our aerial photo analysis successfully separated the collapse due to the first and second events, but it was not clear how the first earthquake changed the fragility of the buildings, i.e., whether the same damage is expected if the second earthquake occurred without the first one. According to the report (Committee to analyze causes of building damage in the Kumamoto earthquake, 2016), the response analysis with the discrete element method showed the wooden structures built after 2000 were expected to collapse for the shaking levels of the April 16 event. Therefore, although the degradation due to the first event was not clear, the second event was strong enough to cause the significant damage.

CONCLUSIONS

We analyzed the aerial photos of Mashiki town taken before and after the two Kumamoto earthquakes that occurred on April 14 and 16 to identify the damage due to the earthquakes. The building damage was concentrated in the town center, especially the northern part of the area between Route 28 and the Akitsu river. The spatial patterns of collapsed buildings from the April 14 and 16 events were quite similar, which suggests that the damage to the wooden buildings was caused by local conditions, such as the seismic performance of the buildings or the subsurface soil structures. Our photo analysis using past aerial photos shows that the older buildings have a higher collapse ratio throughout the area. The cause of the damage heterogeneity was likely not due to an earthquake source effect, but probably due to a combination of the local site conditions and age of buildings.

There is a strong correlation between the age of buildings and collapse ratio. However, the changes in the building code in 1981 and 2000 had smaller effect on the collapse ratio than the aging degradation. The building age seems to have more influence on the seismic performance than the differences in the building code.

Aerial photo analysis is a good method to identify story-collapsed buildings, but it is difficult to identify severely damaged buildings without story collapse. The number of totally collapsed buildings estimated in the photo analysis was about half the number observed from the field survey.

ACKNOWLEDGEMENTS

The authors are grateful to the Kumamoto prefecture and National Research Institute for Earthquake Science and Disaster Resilience, Japan, for providing strong-motion data. We thank the joint team from Kyoto University, NEWJEC Inc., and the Building Research Institute for providing the field survey data and aftershock records. We appreciate valuable comments from Dr. Jim Mori in Kyoto University and anonymous reviewers.

REFERENCES

Aki, K., 1993. Local site effects on weak and strong ground motion. *Tectonophysics* **218**, 93–111.

Asano, K. and Iwata, T., 2016. Source rupture processes of the foreshock and mainshock in the 2016 Kumamoto earthquake sequence estimated from the kinematic waveform inversion of strong motion data. *Earth, Planets and Space* **68**, 147.

Booth, E., Saito, K., Spence, R., Madabhushi, G., and Eguchi, R. T., 2011. Validating assessments of seismic damage made from remote sensing. *Earthquake Spectra* **27**, S157–S177.

Committee to analyze causes of building damage in the Kumamoto earthquake, 2016. Final report.

Foulser-Piggott, R., Spence, R., Eguchi, R., and King, A., 2016. Using Remote Sensing for Building Damage Assessment: GEOCAN Study and Validation for 2011 Christchurch Earthquake. *Earthquake Spectra* **32**, 611–631.

Geological Survey of Japan, 2016. Fourth report: field survey report (May 13, 2016) Surface rupture that appeared for the 2016 Kumamoto Earthquake.

Geological Survey of Japan, AIST, 2017. Geological Maps Download.

Geospatial Information Authority of Japan, 2016a. Information on the 2016 Kumamoto earthquake.

Geospatial Information Authority of Japan, 2016b. Maps and aerial photographs browsing service.

Goda, K., Campbell, G., Hulme, L., Ismael, B., Ke, L., Marsh, R., Sammonds, P., So, E., Okumura, Y., and Kishi, N., 2016. The 2016 Kumamoto Earthquakes: Cascading Geological Hazards and Compounding Risks. *Frontiers in Built Environment* **2**, 19.

Hayashida, T., Yamada, M., Mori, J., Sakaue, H., Yamada, M., Hada, K., Fujino, Y., Fukatsu, S., Nishihara, E., Ouchi, T., and Fujii, A., 2016. Investigation of the Damage Mechanism in the Mashiki-town for the 2016 Kumamoto earthquake: Part 3 Aftershock Observation. *Abstract of the Seismological Society Japan Fall Meeting* .

Idriss, I. and Seed, H. B., 1968. An analysis of ground motions during the 1957 San Francisco earthquake. *Bulletin of the Seismological Society of America* **58**, 2013–2032.

Japan Meteorological Agency, 2016. Information on the 2016 Kumamoto earthquake.

Kunugi, T., 2000. Relationship between Japan Meteorological Agency Instrumental Intensity and Instrumental Modified Mercalli Intensity Obtained from K-NET Strong-motion Data. *Zisin* **53**, 89–93.

Nagaki, A., Araki, S., and Suzuki, Y., 2009. Residential Land Process in Mashiki Town By Spread of Kumamoto urban field –Reading Changes of Land Use by Topographical Map–. *Bulletin of School of Information Business Studies, Tokai University* pp. 51–65.

NIED, 2016. NIED Strong-motion Seismograph Networks (K-NET and KiK-net).

Nishinippon Shimbun Website, 2016. A branch fault leads to damage concentration? *(in Japanese)*.

Okada, S. and Takai, N., 2000. Classifications of structural types and damage patterns of buildings for earthquake field investigation. *Proceedings of the 12th world conference on earthquake engineering (paper 0705), Auckland* .

Shirahama, Y., Yoshimi, M., Awata, Y., Maruyama, T., Azuma, T., Miyashita, Y., Mori, H., Imanishi, K., Takeda, N., and Ochi, T., 2016. Characteristics of the surface ruptures associated with the 2016 Kumamoto earthquake sequence, central Kyushu, Japan. *Earth, Planets and Space* **68**, 191.

Wen, K.-L., Beresnev, I. A., and Yeh, Y. T., 1994. Nonlinear soil amplification inferred from downhole strong seismic motion data. *Geophysical Research Letters* **21**, 2625–2628.

Yagi, Y., Okuwaki, R., Enescu, B., Kasahara, A., Miyakawa, A., and Otsubo, M., 2016. Rupture process of the 2016 Kumamoto earthquake in relation to the thermal structure around Aso volcano. *Earth, Planets and Space* **68**, 118.

Yamada, M., Mori, J., Sakaue, H., Hayashida, T., Yamada, M., Hada, K., Fujino, Y., Fukatsu, S., Nishihara, E., Ouchi, T., and Fujii, A., 2016a. Investigation of the Damage Mechanism in the Mashiki-town for the 2016 Kumamoto earthquake: Part 1 Building Damage Survey. *Abstract of the Seismological Society Japan Fall Meeting* .

Yamada, M., Yamada, M., Mori, J., Sakaue, H., Hayashida, T., Hada, K., Fujino, Y., Fukatsu, S., Nishihara, E., Ouchi, T., and Fujii, A., 2016b. Investigation of the Damage Mechanism in the Mashiki-town for the 2016 Kumamoto earthquake: Part 2 Microtremor Observation. *Abstract of the Seismological Society Japan Fall Meeting* .

Table 1. Error matrix of the damage level from the field survey and photo analysis.

		Field survey				Total
		D0	D1-D3	D4	D5	
Photo analysis	standing	371	222	136	79	808
	collapsed	0	9	22	202	233
Total		371	231	158	281	1041

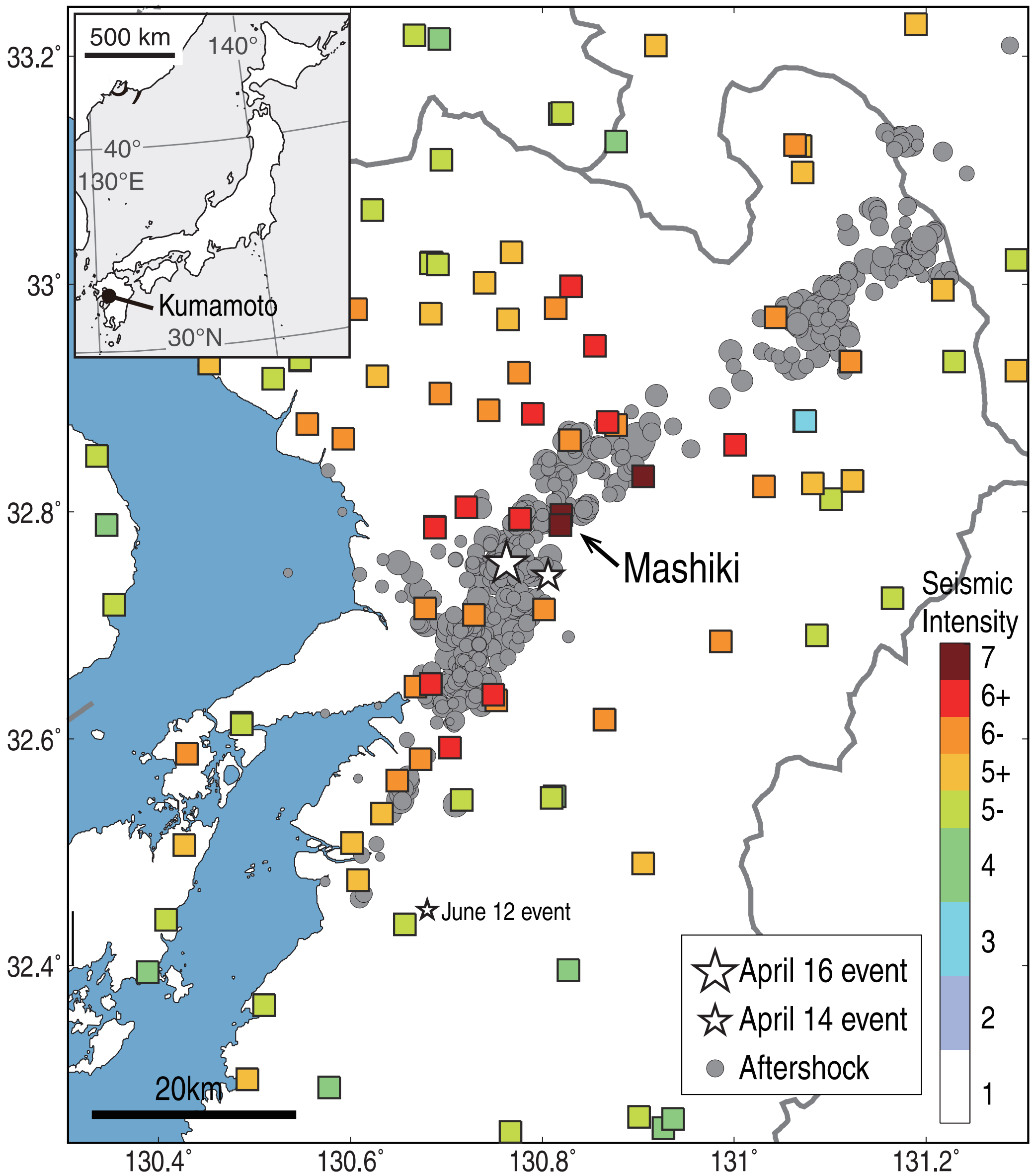

Figure 1. JMA seismic intensity (colored squares) for the April 16 event and aftershock distribution on April 16, 2016 (gray circles). The stars show the epicenters of the April 14, 16 and June 12 events.

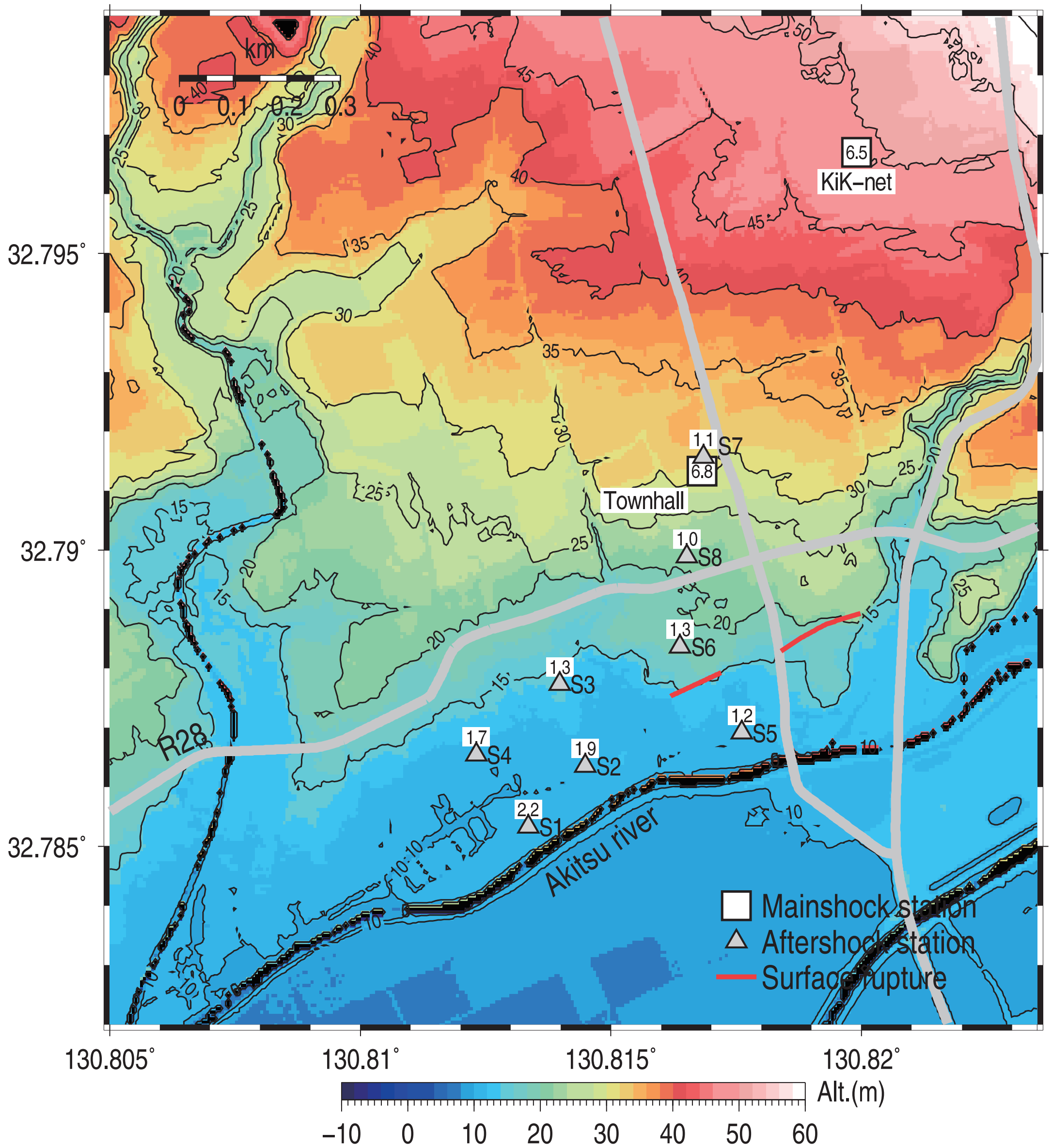

Figure 2. Topographic map of Mashiki town with JMA seismic intensity of April 16 event (square symbols) and aftershock on June 12 (triangle symbols). The red lines show the surface rupture (Geological Survey of Japan, 2016).

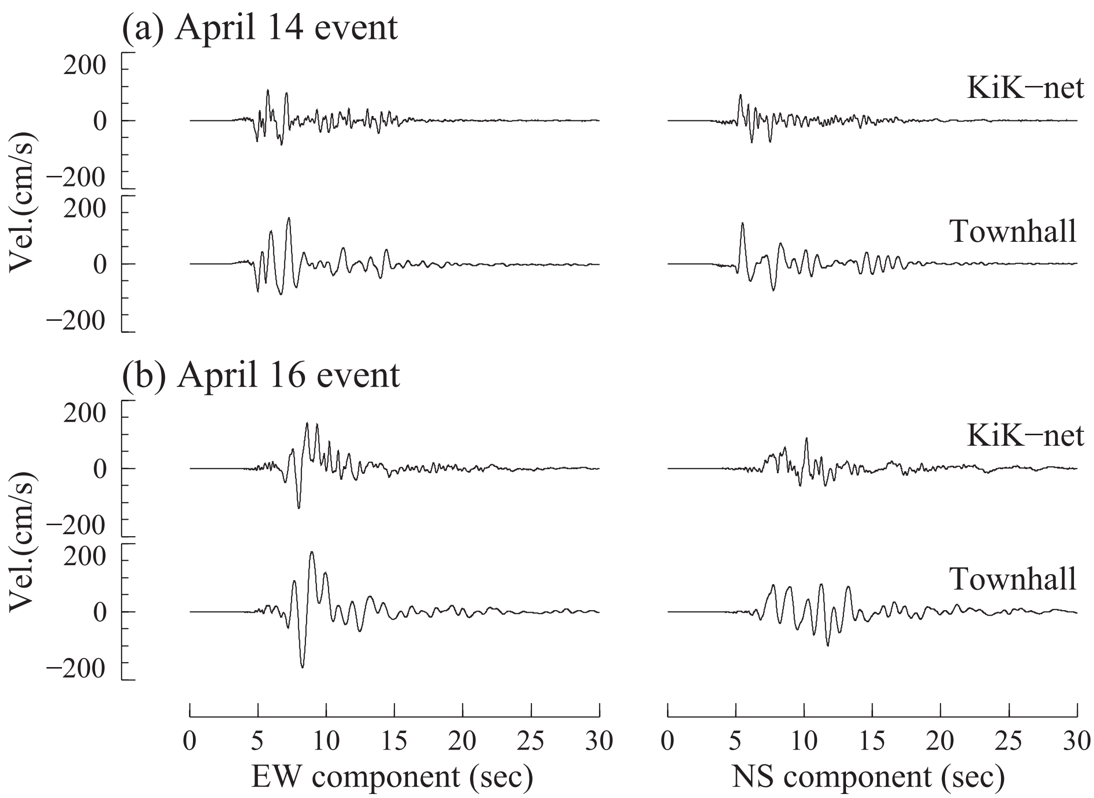

Figure 3. Velocity waveforms for (a) April 14 and (b) April 16 event. Locations of the stations are shown in Figure 2.

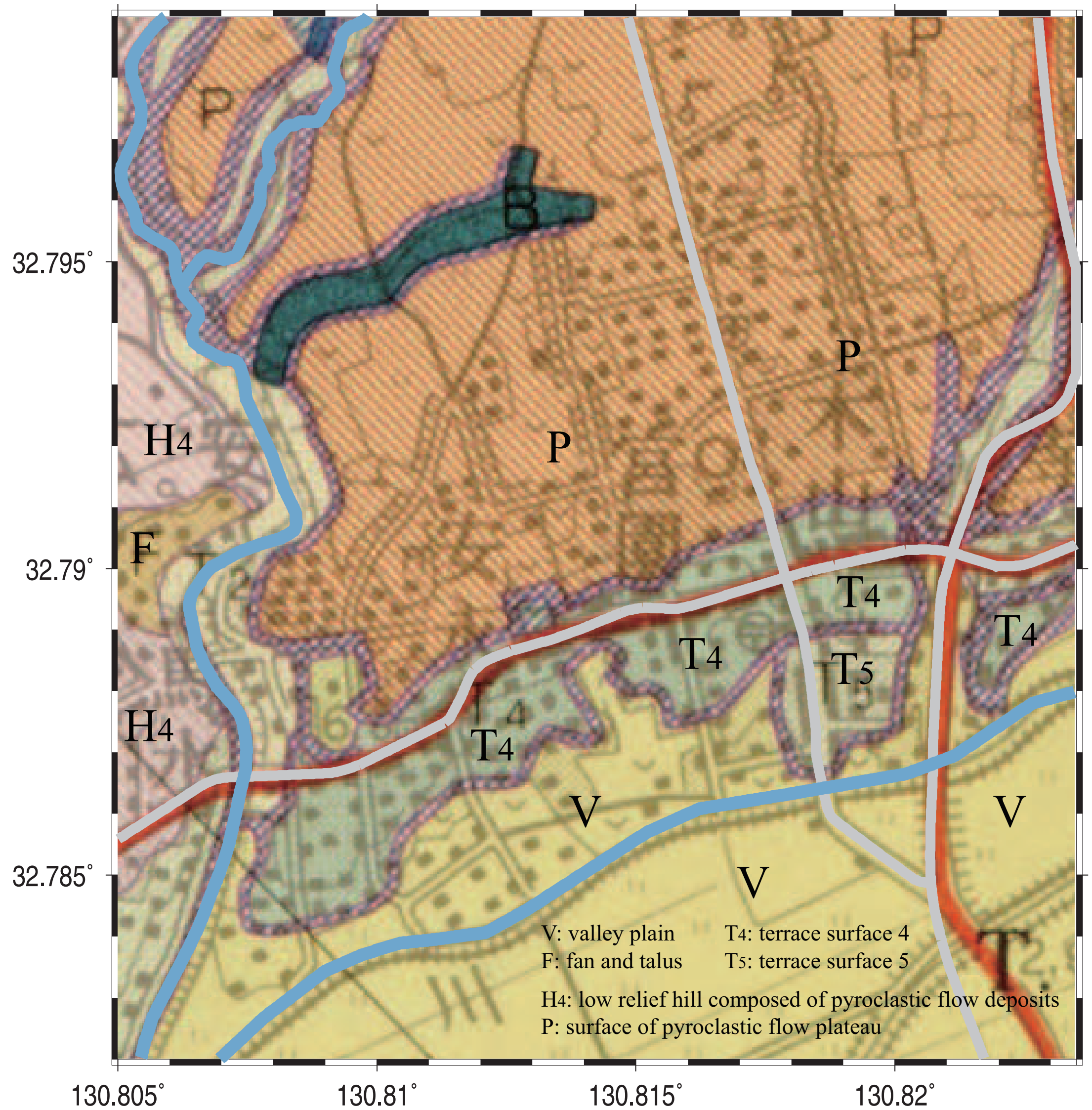

Figure 4. Geomorphological map of Mashiki town (Geological Survey of Japan, AIST, 2017).

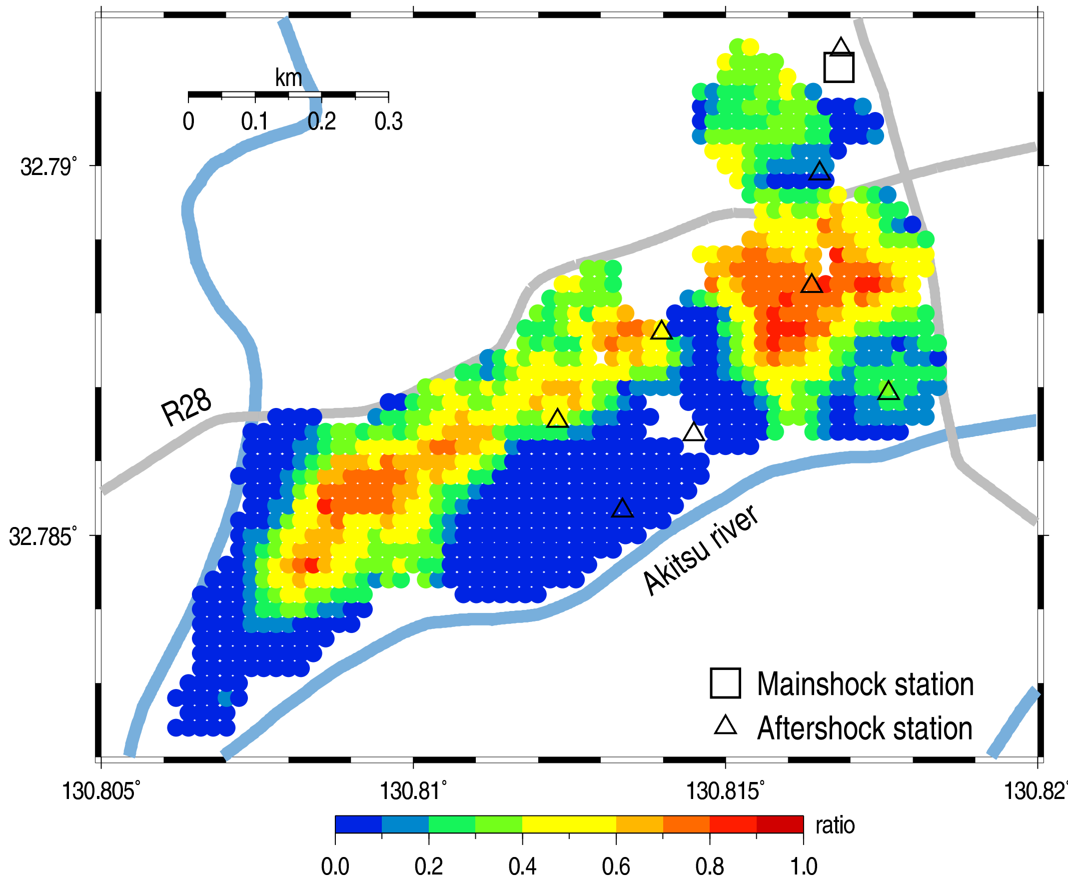

Figure 5. Ratio of D5 (story-collapsed) wooden buildings detected from the field survey conducted in June 2016. The square and triangle symbols are the same stations as those indicated in Figure 2.

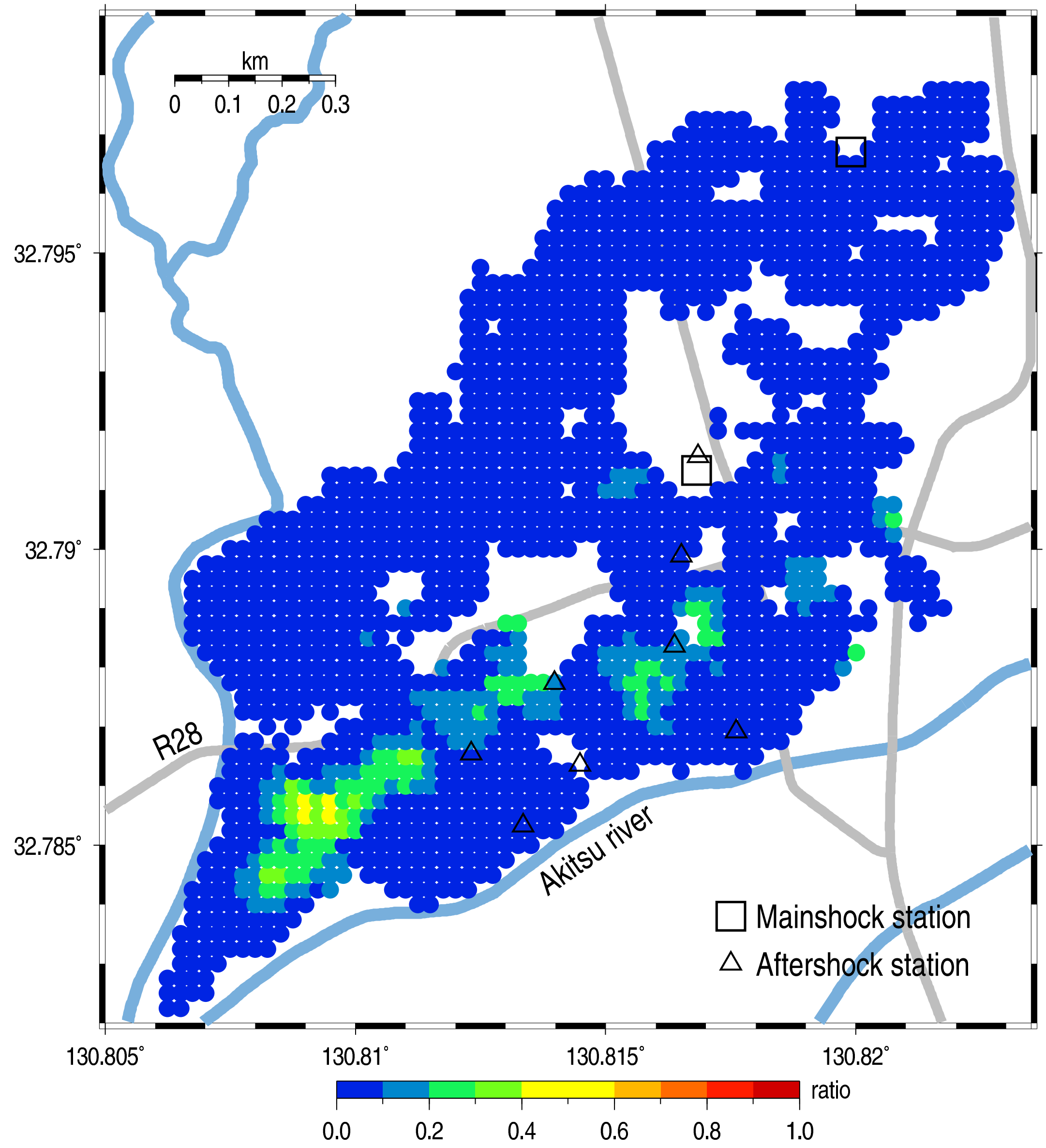

Figure 6. Ratio of collapsed buildings detected from the aerial photo analysis before the April 16 event. The square and triangle symbols are the same stations as those indicated in Figure 2.

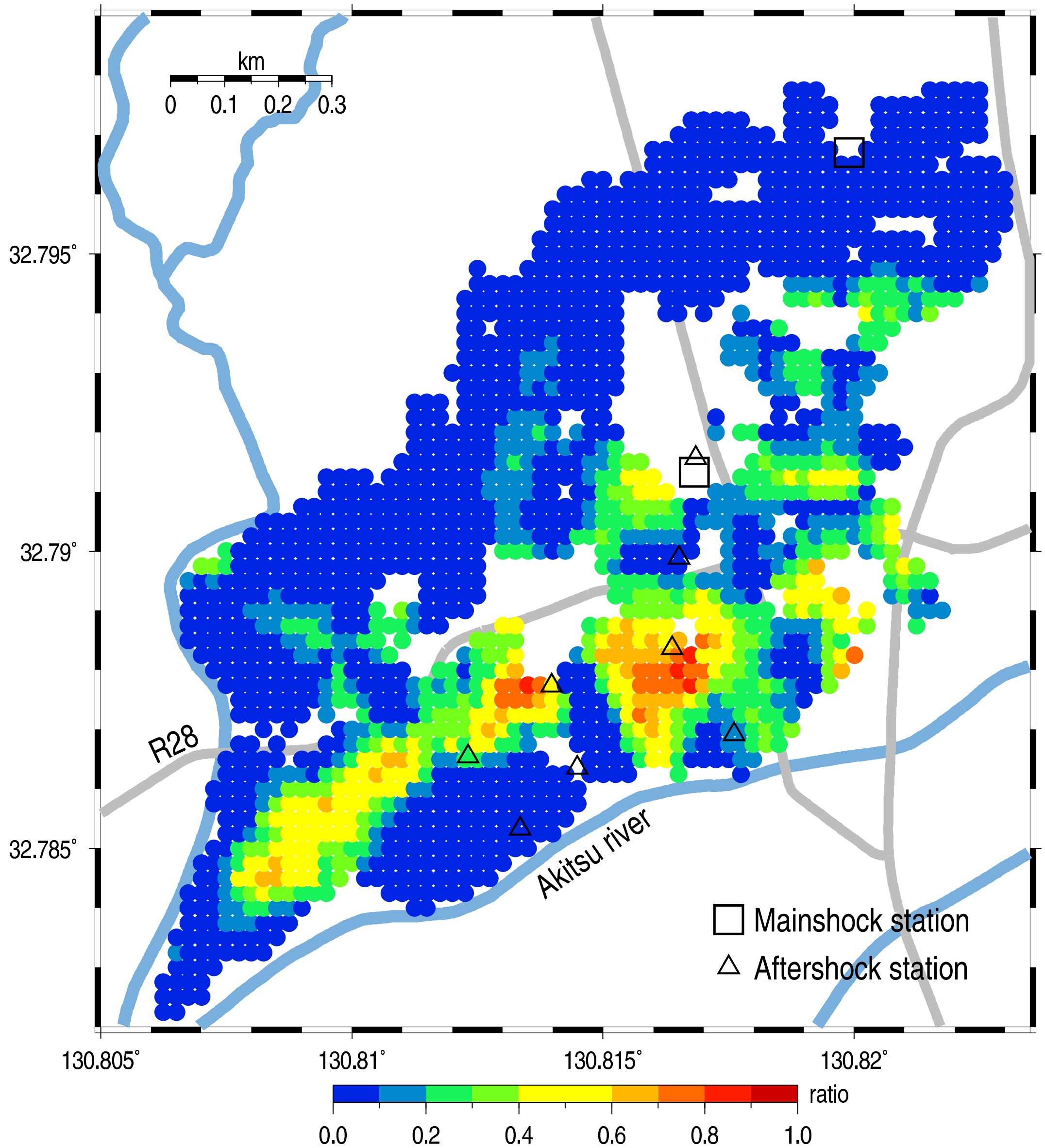

Figure 7. Ratio of collapsed buildings detected from the aerial photo analysis after the April 16 event. The square and triangle symbols are the same stations as those indicated in Figure 2.

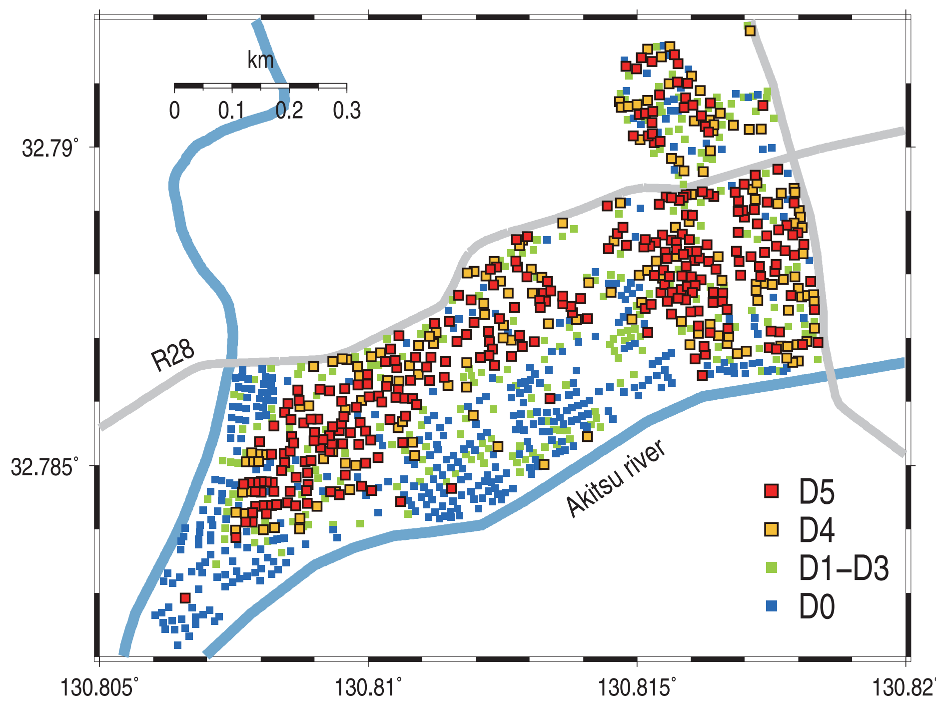

Figure 8. Distribution of damaged buildings detected from the field survey conducted in June 2016. Colors show the damage level.

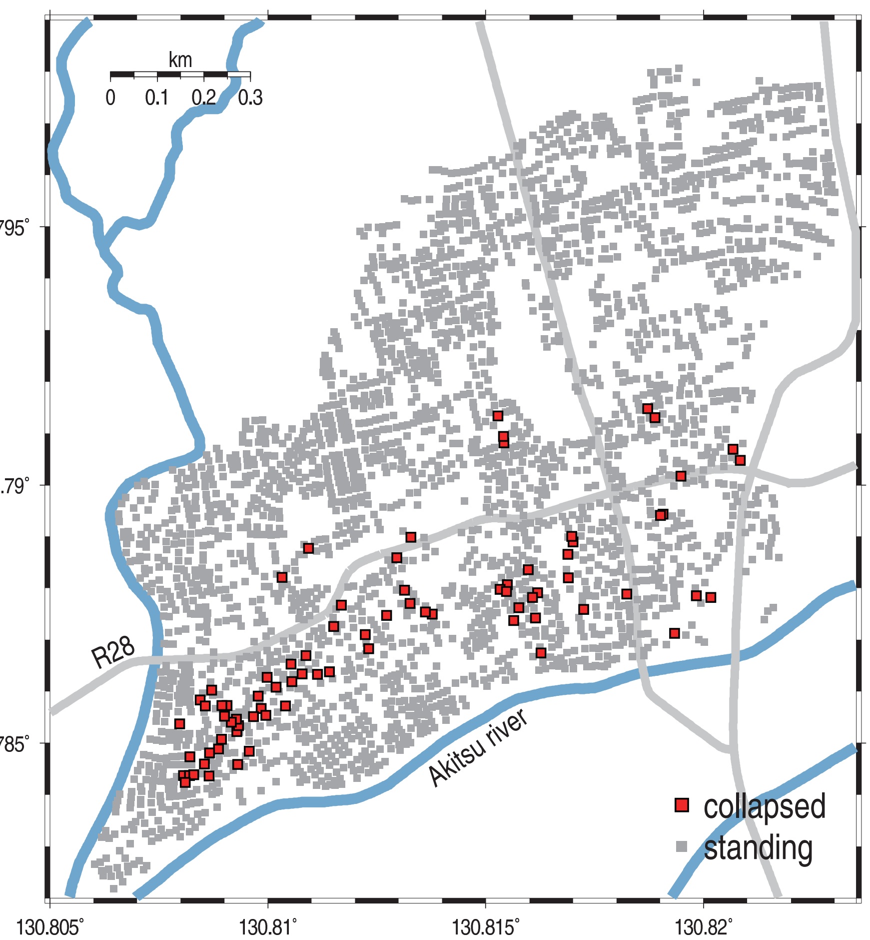

Figure 9. Distribution of collapsed buildings detected from the aerial photo analysis before the April 16 event.

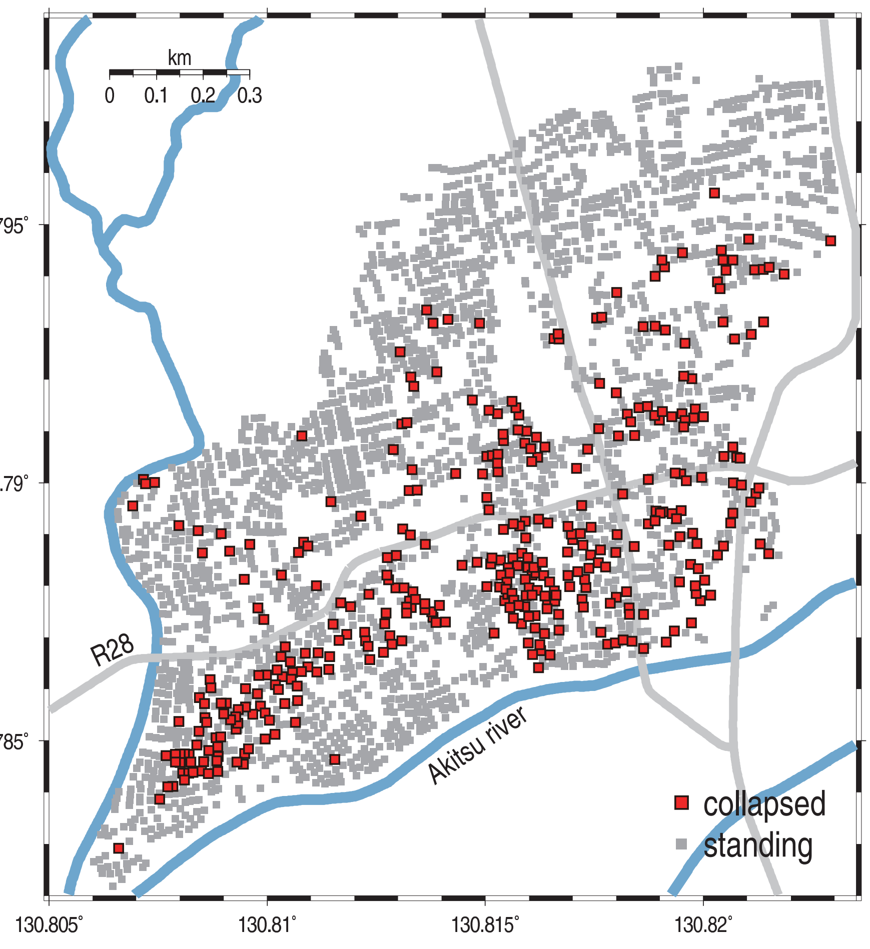

Figure 10. Distribution of collapsed buildings detected from the aerial photo analysis after the April 16 event.

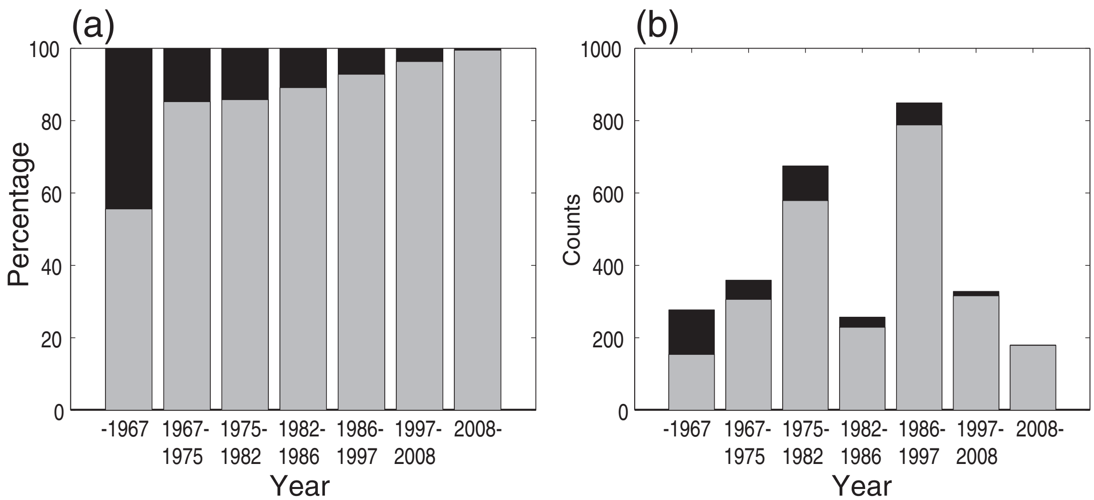

Figure 11. (a) Percentage and (b) number of collapsed buildings (black) and standing buildings (gray) for different building construction periods.

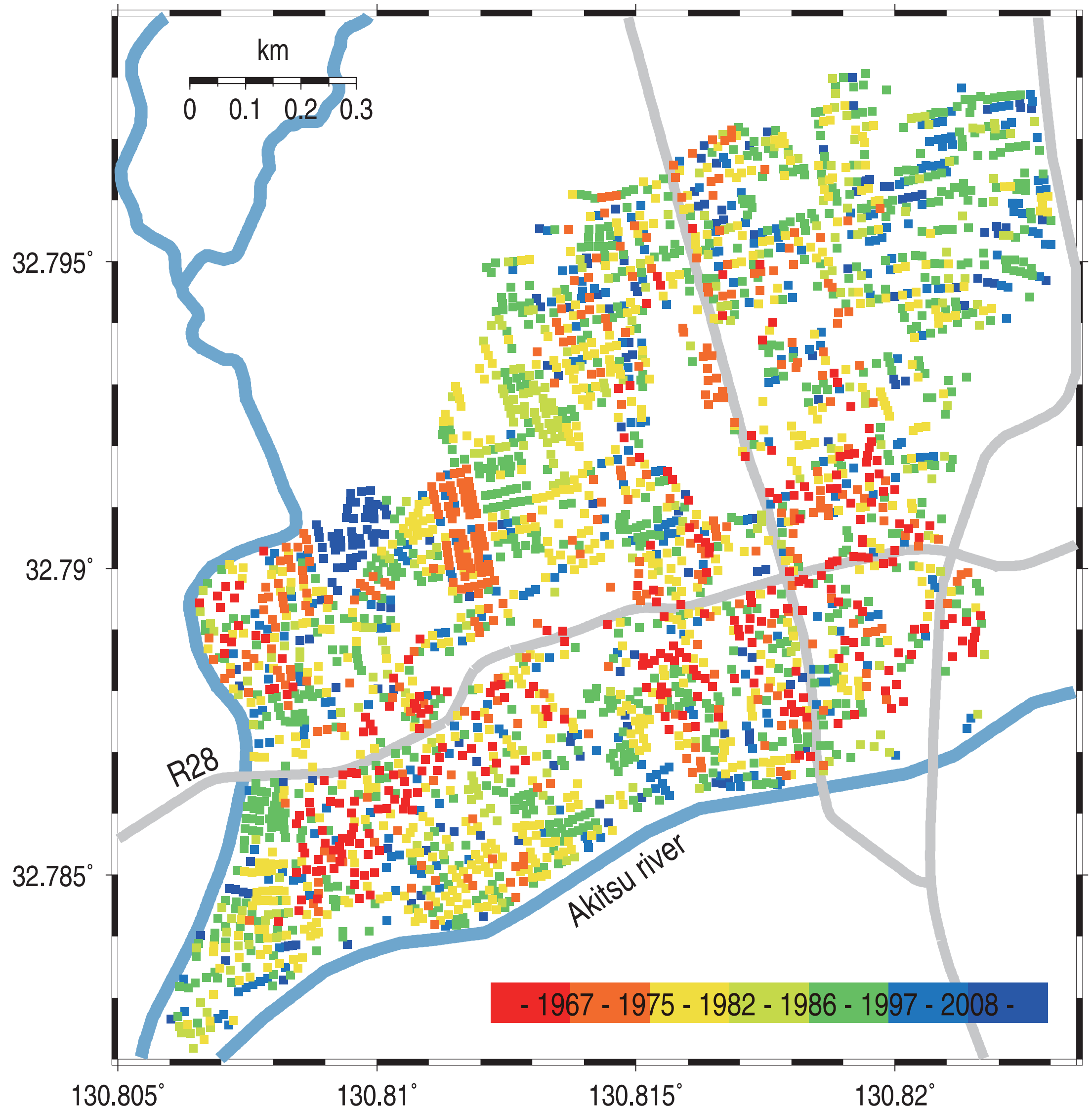

Figure 12. Age of buildings detected from the aerial photo analysis. Colors show the construction periods.

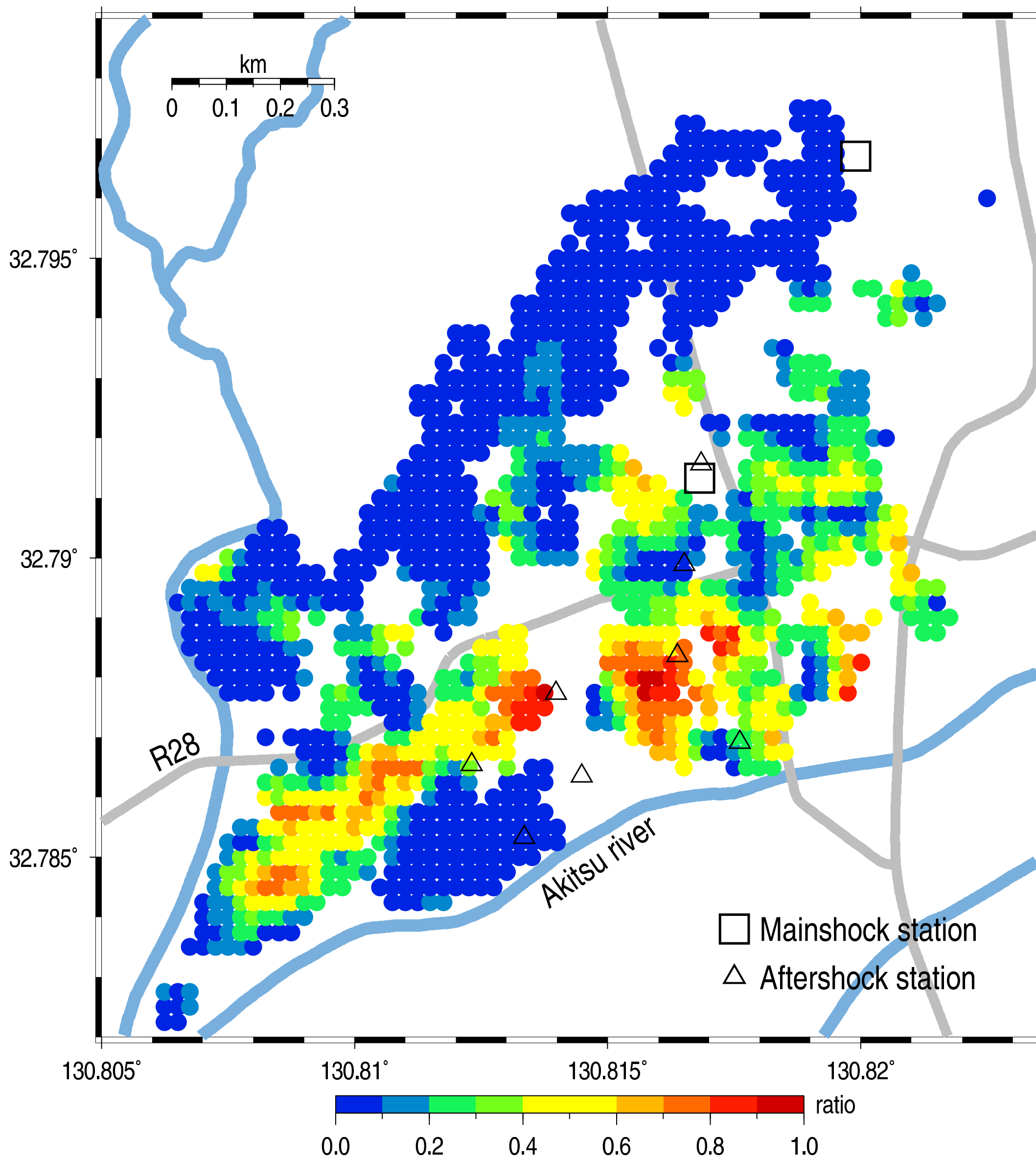

Figure 13. Ratio of collapsed buildings that were constructed between 1967 and 1986, detected from the aerial photo analysis after the April 16 event.

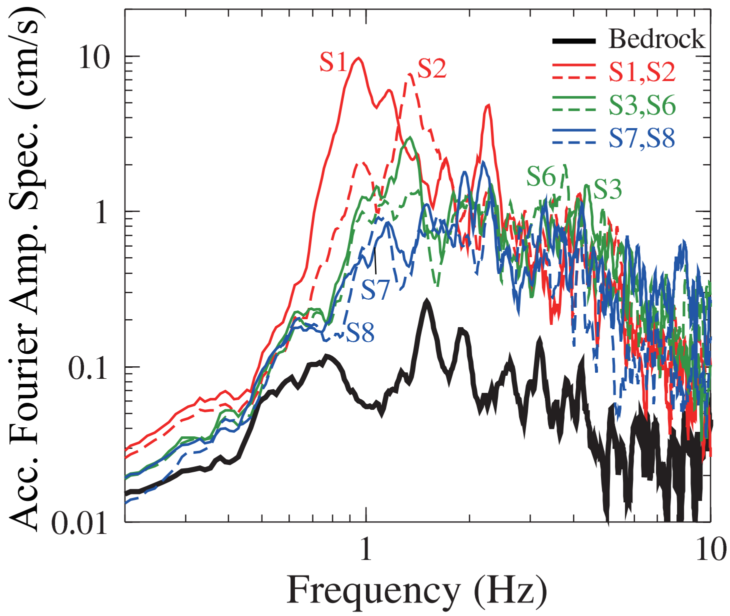

Figure 14. Fourier amplitude spectrum of EW component for the aftershock. Black line shows the KiK-net borehole record, and colored lines show the records at temporal stations shown in Figure 2.

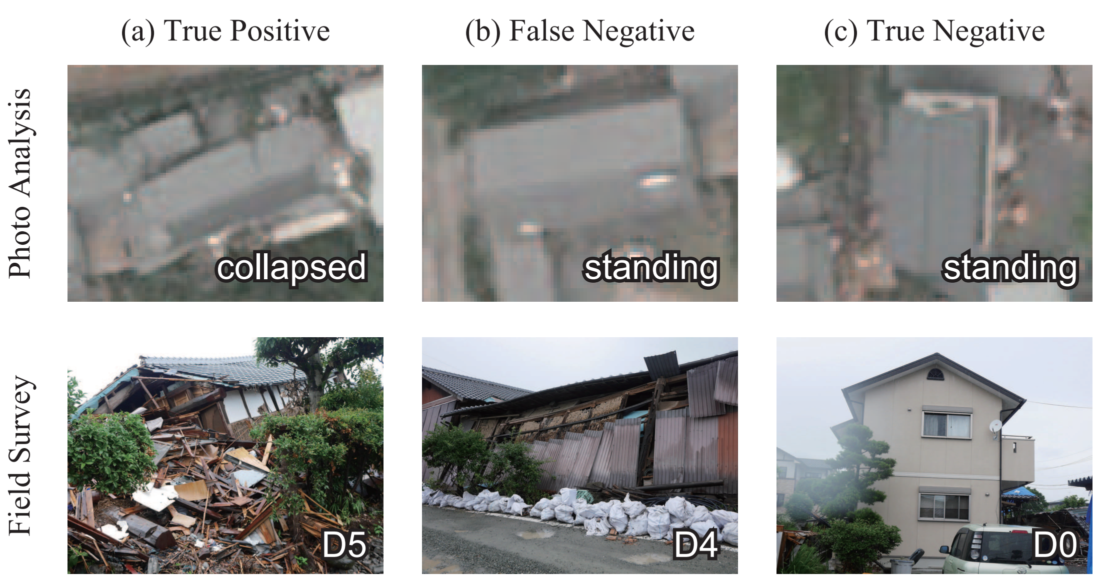

Figure 15. Examples of the (a) true positive, (b) false negative, and (c) true negative of the damage level from the photo analysis and field survey.